Unveiling the Mysteries: Acetonitrile's Dance with Weakly-Solvating Electrolytes in Shaping Gas Evolution and Electrochemical Performance of

How to cite: Angew. Chem. Int. Ed. 2024, e202402206
doi.org/10.1002/anie.202402206

Batteries

Unveiling the Mysteries: Acetonitrile's Dance with Weakly-Solvating Electrolytes in Shaping Gas Evolution and Electrochemical Performance of Zinc-ion Batteries

*Zhenrui Wu[+], Yihu Li[+], Amardeep Amardeep[+], Yijia Shao, Yue Zhang, Jian Zou, Liping Wang, Jia Xu, Dawid Kasprzak, Evan J. Hansen, and Jian Liu**

Abstract: Aqueous Zn-metal battery (AZMB) is a promising candidate for future large-scale energy storage with commendable capacity, exceptional safety characteristics, and low cost. Acetonitrile (AN) has been widely used as an effective electrolyte constituent to improve AZMBs' performance. However, its functioning mechanisms remain unclear. In this study, we unveiled the critical roles of AN in AZMBs via comparative in situ electrochemical, gaseous, and morphological analyses. Despite its limited ability to solvate Zn ions, AN-modulated Zn-ion solvation sheath with increased anions and decreased water achieves a weakly-solvating electrolyte. As a result, the Zn||Zn cell with AN addition exhibited 63 times longer cycle life than cell without AN and achieved a 4 Ah cm^{-2} accumulated capacity with no H_2 generation. In V_2O_5||Zn cells, for the first time, AN suppressing CO_2 generation, elevating CO_2-initiation voltage from 2→2.44 V (H_2: 2.43→2.55 V) was discovered. AN-impeded transit and Zn-side deposition of dissolved vanadium ions, known as "crosstalk," ameliorated inhomogeneous Zn deposition and dendritic Zn growth. At last, we demonstrated an AN-enabled high-areal-capacity AZMB (3.3 mAh cm^{-2}) using high-mass-loading V_2O_5 cathode (26 mg cm^{-2}). This study shed light on the strategy of constructing fast-desolvation electrolytes and offered insights for future electrolyte accommodation for high-voltage AZMB cathodes.

Introduction

The increasing demand for efficient and durable large-scale energy storage solutions has driven extensive research into advanced battery technologies. Among these, aqueous Zn-metal batteries (AZMBs) have garnered significant attention due to their cost-benefit, safety characteristics, and resource availability.[1] Particularly, aqueous electrolytes are non-toxic and non-flammable, and Zn metal has an exceptional capacity of 5,855 mAh cm^{-3}.

Despite the decent compatibility of Zn metal with water, the relatively high reactivity of water at the electrode-electrolyte interface creates several issues, such as unstable solid-electrolyte interphase (SEI) formation, hydrogen (H_2) evolution, Zn dendrite formation, Zn corrosion/passivation, and cathode dissolution,[2] leading to the inferior performance of AZMBs. In addition, challenges of aqueous electrolytes, such as the limited electrochemically stable potential window (ESPW) and thermal stability window (TSW), exist. The ESPW is determined by multiple factors, such as the selection of salt and solvent, concentration of salt, *etc.* Particularly, the ESPW of 1 M $ZnSO_4$ and $Zn(OTf)_2$ aqueous electrolytes can reach 2.3 and 2.4 V (vs. Zn^{2+}/Zn), respectively.[3] The TSW of an electrolyte is closely related to its selection of solvent. The emerging electrolytes with excellent TSW in AZMBs are often not entirely aqueous and are prepared with the participation of wide-TSW solvents, such as deeply eutectic solvents (DESs),[4] ionic liquids (ILs),[5] and conventional organic solvents.[6] Using organic-aqueous hybrid solvents is expected to improve both the ESPW and TSW without compromising the ionic conductivity of aqueous system and electrochemical reac-

[*] Z. Wu,[+] A. Amardeep,[+] Y. Shao, Y. Zhang, J. Xu, D. Kasprzak, E. J. Hansen, Dr. J. Liu
School of Engineering, Faculty of Applied Science, The University of British Columbia, Kelowna, V1 V 1 V7, Canada
E-mail: jian.liu@ubc.ca

Y. Li[+]
Department of Physics, Chalmers University of Technology, Göteborg, SE-41296 Sweden

Y. Shao
The Key Laboratory of Fuel Cell Technology of Guangdong Province & The Key Laboratory of New Energy, School of Chemistry and Chemical Engineering, South China University of Technology, Guangzhou 510641, China

J. Zou, L. Wang
School of Materials and Energy, University of Electronic Science and Technology of China, Chengdu, 611731, China

D. Kasprzak
Institute of Chemistry and Technical Electrochemistry, Poznan University of Technology, Berdychowo 4 St., 60-965, Poznan, Poland

[+] These three authors share equal contributions.

tivity of cathode materials.[7] For instance, 1,3-dioxolane (DOL)/H_2O hybrid solvent can expand the ESPW of the electrolyte to 4.7 V (vs. Zn^{2+}/Zn) and TSW to as low as −50 °C.[8]

The development of AZMBs is contingent upon a deep understanding of the intricate interactions between electrode materials and electrolytes as well as the dominant and parasitic electrochemical and chemical processes occurring within the cell. Previous studies have developed multiple strategies to modify the solvation structure of Zn ions and ameliorate these issues associated with high water reactivity. To be more exact, reducing the amount of water in the Zn-ion solvation sheath can prohibit water-related side reactions at the interface, such as H_2 generation, followed by a local pH change that leads to Zn corrosion and passivation. Modifying the solvation structure also influences the kinetics of Zn-ion desolvation, which determines the flux of arriving Zn^{2+} on the Zn metal anode and the homogeneity of Zn deposition.[9] The reduction of solvating water also indirectly increases the number of anions or organic molecules in Zn solvates, whose first-cycle decomposition is expected to introduce an inorganic or organic layer of SEI, stabilizing the interface and, thus, prohibiting further parasitic reactions.[10]

The modification of Zn-ion solvation sheath can be achieved in three ways. (i) The first way is to restrain the relative amount of water vs. Zn ions. For example, a super-concentrated electrolyte, also known as a water-in-salt electrolyte (WiSE), significantly reduces the amount of water in Zn-ion solvation[11] and increases the chance of SEI formation,[12] which macroscopically leads to an expanded ESPW; however, their costly chemistry and high viscosity at low temperatures hinder their commercialization. Later, a localized high-concentration electrolyte (LHCE) can be achieved by diluting WiSE into a non-polar diluent, also called a "non-solvent." In this way, the solvation structure is preserved while the cost and viscosity of the electrolyte are much reduced. However, achieving an LHCE for AZMBs is challenging. So far, the most soluble salt, $ZnCl_2$, presents flaws because the instability of Cl^- can cause persistent side reactions. As a result, 1 M $ZnCl_2$ electrolytes show a narrow ESPW of 0.75 V (vs. Zn^{2+}/Zn),[13] while the selection of diluent remains incomprehensible.[14] (ii) The second is to introduce an organic co-solvent into the Zn-ion solvation sheath. The co-solvent should possess a comparable Gutmann donor number (DN) to water (e.g., methanol (MeOH),[15] dimethylacetamide (DMA),[16] dimethyl sulfoxide (DMSO),[17] triethyl phosphate (TEP),[18] ethylene glycol (EG)),[19] demonstrating their nucleophilic ability to metal ions, as well as a high dielectric constant (ε), indicating their strong solubility in polar water. By occupying the positions of water within the solvation sheath of Zn ions, the approach can mitigate undesirable side reactions stemming from electrode-water interfacial instability and introduce organic components in SEI from the decomposition of these co-solvents. However, the stronger coordination between Zn ions and these high-DN organics leads to more sluggish desolvation kinetics, resulting in uneven Zn^{2+} flux from the outer Helmholtz layer to the Zn anode, which is, unfortunately, the intrinsic cause of dendritic Zn growth.[20] (iii) The third is by introducing additives that can weaken the solvating power of H_2O to realize a weakly-solvating electrolyte (WSE). The benefit of WSE is to lessen active water in Zn solvates and reduce water-induced parasitic reactions. The anions in the solvation sheath are easy to be desolvated due to the electrostatic repulsion from the negatively charged Zn metal anode, leading to fast desolvation kinetics. Sufficient Zn^{2+} reflux helps ameliorate the uneven Zn deposition.[21] Theses additives can be either bulky organic molecules with strong water affinity, known as "crowding" agents (e.g., PEG-400,[22] PEGDME),[23] or small hydrophilic (high ε) molecules with low DN (e.g., PC,[24] DEC,[25] butanone).[20] The crowding agents can break hydrogen bonds (HBs) and construct cages for water molecules, thereby reducing water's solvating power with Zn ions and squeezing more anions into the solvation sheath. However, introducing crowding agents may harm the ionic conductivity. On the other hand, small hydrophilic molecules function similarly to the big-molecule crowding agents in forming a water-deficient solvation structure of Zn ions and achieving a wide ESPW without sacrificing ionic conductivity.

Using acetonitrile (AN) as the only solvent in non-aqueous electrolytes for Zn batteries was first explored in 2018 (Figure S1). Nazar et al.[26] reported the rate performance of $V_3O_7{\cdot}H_2O$/Zn cells constructed with 0.25 M Zn-$(OTf)_2$-AN electrolyte significantly worse than that with 1 M $ZnSO_4$–H_2O electrolyte owing to (i) the large radii of Zn^{2+}–AN solvates impeded co-insertion, in contrast with Zn^{2+} partly co-inserted to the cathode with water; (ii) the chemisorbed H_2O on cathode and H_2O in electrolyte formed half-solid half-liquid coordination conducive to fast Zn-ion diffusion. Later studies reported the utility of AN as an additive in aqueous electrolytes, improving Zn reversibility through a surface absorption mechanism[27] and enhancing full-cell cycling stability[28] by forming stable electrode-electrolyte interphases.[29] For example, in 2020 Tao et al.[27] investigated the low-concentration $Zn(OTf)_2$–AN/H_2O hybrid system and achieved an enhanced Zn reversibility and cycling stability in vanadium pentoxide (V_2O_5)||Zn full cells by adjusting the ratio of AN and H_2O to 1:3 (by vol.). Wei et al.[29] optimized the AN/H_2O ratio to 1:0.6 (by mol.) and observed a correlation of "small water ratio—high pH—long activation time." However, their AN/H_2O ratio adjustments were confined to Zn||Zn configuration, and the suitability of pH-based criteria for non-aqueous electrolyte remains under debate. In 2021, Liu et al.[30] extended the utilization of AN/H_2O to ultra-high-concentration systems and developed an AN/water-in-salt (AWiS) electrolyte for MnO_2|15 M $Zn(OTf)_2$-AN/H_2O (1:1 by vol.)|Zn with a widened ESPW, yet substantial room for enhancing the battery's cycling stability remains.

Despite past endeavors exploring the use of AN as the only solvent or additive in Zn-based electrolytes, the formation of gaseous byproducts from interfacial side reactions remains a subject warranting deeper understanding. Many studies have observed bubble formation in Zn||Zn cells using in situ optical microscopy (OM).[31] These

bubbles were generated due to water reduction reaction, a parasitic reaction alongside Zn^{2+}/Zn, and have been identified as H_2 by differential electrochemical mass spectrometry (DEMS)[32] or gas chromatography–mass spectrometry (GC-MS).[33] However, understanding of gassing phenomena in full cells, especially at the cathode side, is lacking. Direct observation regarding gas evolution and its association with dendritic Zn growth, a crucial aspect for comprehensively understanding the efficacy of any functional additive, co-solvent, or non-solvent, is also lacking. The root cause of the improved full-cell cycling with AN and its implications are yet to be established.

This study aims to elucidate the fundamental mechanisms and electrochemical effects of AN additive in $V_2O_5||$Zn batteries by employing in situ DEMS and OM techniques. The concurrent use of these techniques revealed critical electrochemical improvements resulting from the use of AN, such as reducing gas generation, mitigating cathode dissolution, and suppressing the crosstalk phenomenon of V ions in $V_2O_5||$Zn full cells, providing foundational insights into the capabilities of AN as the electrolyte additive. The interaction between AN and the various components of the battery, including the anode, cathode, and electrolyte, is explored to understand comprehensively how this additive influences the overall cell performance. A thermodynamic viewpoint of the gas evolution is presented and offers a basis for addressing short-circuit phenomena in AZMBs. Furthermore, in response to industry requirements for high electrode mass loadings, we delve deeper into the diverse effectiveness of AN under varying positive electrode loadings. A solvent-free dry-film method using polytetrafluoroethylene fibrillation is employed to prepare ultra-high-loading V_2O_5 cathodes up to 26 mg cm^{-2}. Ultimately, the knowledge gleaned from this research can potentially advance AZMBs into a robust and sustainable energy storage solution for renewable energy integration.

Results and Discussions

Unveiling Zn-ion Solvation Structure via MD & FTIR

The optimization of AZMB efficiency critically hinges upon meticulous management of side reactions transpiring within the Zn-ion solvation sheath. Inherent to the relatively low lattice energy of $Zn(OTf)_2$ crystal, its solubility in either water or AN is appreciable. However, due to the low DN of AN (14.1 kcal mol^{-1})[34] compared with water (18 kcal mol^{-1}), AN with insufficient nucleophilic ability is an unfavorable solvating agent in an AN/H_2O mixed system. The chemical structure of each electrolyte constituent and the electrostatic potentials (ESP) of AN vs. water are provided in Figure 1a–b. More physiochemical properties are summarized in Table S1.

Through a molecular dynamics (MD) method, we computationally investigated the coordination structure of Zn-ion solvation sheaths in a water-only system (3-A_0H_1, Figure 1c) and an AN/H_2O-mixed system (3-A_1H_1, Figure 1d). Details of the calculation method are provided in the experimental section of the supporting document. From that, we calculated the radical distribution function (RDF) and the average coordination number (ACN) of each constituent of these solvation sheaths (Figure 1e–f). The ACN of water to Zn ion was reduced from 4.88 (3-A_0H_1) to 4.23 (3-A_1H_1), while the ACN of OTf^- to Zn ions was increased from 0.40 to 0.44. We also conducted a statistical analysis on all Zn-solvate forms observed in the two electrolytes (Figure S2, Table S2). It turned out that 34 % of Zn ions in 3-A_0H_1 exist as $[Zn^{2+}(H_2O)_6]$ and 35 % as $[Zn^{2+}(OTf^-)_1(H_2O)_5]$, while the dominant Zn^{2+}-solvate form in 3-A_1H_1 manifests as $[Zn^{2+}(OTf^-)_2(H_2O)_4]$ (40 %) and $[Zn^{2+}(OTf^-)_1(H_2O)_5]$ (28 %). Therefore, although AN did not directly solvate with Zn ions due to its lower DN than water, it effectively weakened the solvating ability of water in 3-A_1H_1, leading to a decreased number of water and increased number of the anion within the solvation sheath of Zn ions, i.e., more contact ion pairs (CIPs) and fewer solvent-separated ion pairs (SSIPs) in the form of $[Zn^{2+}(H_2O)_6]$ as AN was mixed into an aqueous electrolyte, summarized in Figure S3.

The molecular vibrational characteristics of $Zn(OTf)_2$, AN, water, and their mutual interactions are revealed by Fourier-transform infrared spectroscopy (FTIR), and the results are presented in Figure 1g. In particular, focusing on pure-phase investigations, water demonstrates characteristic O–H stretching peaks in the range of 3200–3400 cm^{-1}, with the presence of HBs elongating the O–H bonds, resulting in a red shift towards lower wavenumbers. A trace amount of water within $Zn(OTf)_2$-only evokes exceedingly weak O–H stretching signals in the range of 3500–3600 cm^{-1} due to the pronounced isolation of water molecules, resulting in the loss of HBs and a signal of O–H resembling alcohols. The spectra of 3-A_0H_1, 3-A_1H_1, and water suggested that both AN and Zn salt can perturb the HB inherent in water. The blue shift of the O–H stretching peak in 3-A_0H_1 indicates the presence of $H_2O\rightarrow Zn^{2+}$ coordination. In 3-A_1H_1, AN, a high-ε solvent, disrupts the HBs among water molecules, causing a blue shift in O–H stretching vibrations.

AN exhibits characteristic C≡N stretching peaks at around 2250 cm^{-1} and a combination peak of C–C stretching and CH_3 bending at approximately 2300 cm^{-1}.[35] The dipole-dipole interaction between AN and H_2O causes a blue shift of the C≡N bond signal from its initial position to 2255–2260 cm^{-1}, while the concentration of Zn salt presented little impact on C≡N signal (Figure S4). The Zn^{2+}-induced electron-withdrawing effect also prompts a blue shift in the C–C stretching, relocating the original combined peak from 2300 cm^{-1} to 2320 cm^{-1}. A new signal emerges near 2290 cm^{-1}, corresponding to the C≡N stretching of AN confined electrostatically in Zn-solvate aggregate where it is forced to interact with Zn ions,[36] which is observed in the MD simulation result and partially due to the relative strong binding energy of Zn^{2+}–AN (−6.1 eV, Figure S5). In addition, the characteristic vibrations of $Zn(OTf)_2$ salt predominantly manifest in its organic-anion moiety, with peaks below 1300 cm^{-1} in the fingerprint region.[37] The $-CF_3$ in 3-A_0H_1 presents a significant red shift due to the influence of the induction effect of neighboring H_2O, while in 3-A_1H_1,

a more substantial deviation is manifested due to the posterior presence of AN to $–CF_3$. The S=O in $–SO_3$ is also slightly influenced by the solvating agent, water, and presents a redshift to lower wavenumber when dissolved

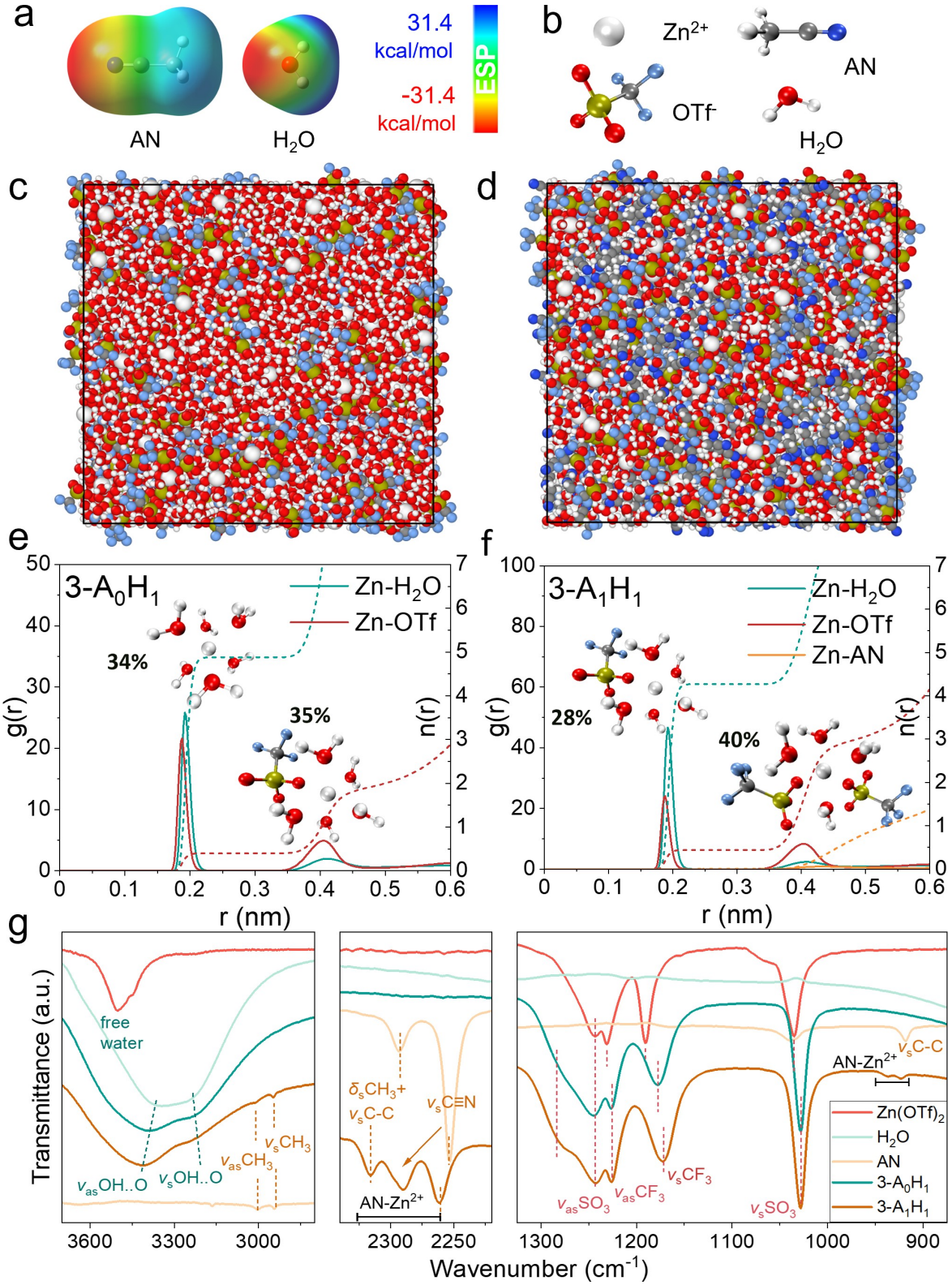

Figure 1. (a) Electrostatic potential of AN and H_2O molecules. (b) Chemical structure of each constituent (i.e., Zn^{2+}, OTf^-, AN, H_2O) of electrolyte. Snapshot of the bulk structure of (c) 3-A_1H_1 and (d) 3-A_0H_1. Radical distribution function (RDF) average coordination number (ACN) from the MD simulation of (e) 3-A_1H_1 and (f) 3-A_0H_1. (g) FTIR spectra of two electrolytes and each constituent $Zn(OTf)_2$, H_2O, and AN.

into either electrolyte. In summary, the addition of AN reduces the H_2O number and increases the OTf^- number in the primary sheath of the Zn-ion solvation structure, while AN itself does not participate in the solvation sheath of any Zn ions but indirectly binds Zn solvates into aggregates.

AN Improves Zn Reversibility and Suppresses H_2 Evolution

AN's improvement of Zn reversibility is verified in both Zn||Zn symmetric cells and Cu||Zn asymmetric cells. Zn||Zn cells prepared with two electrolytes of 3-A_0H_1 and 3-A_1H_1 underwent cycling tests under conditions of 0.5 mA cm^{-2} and 0.5 mAh cm^{-2} until short-circuit (or open-circuit) occurs. As shown in Figure 2a, Zn||Zn cells possess cycling lifespans of 125 and 7,900 hours for 3-A_0H_1 and 3-A_1H_1, respectively. The AN addition in the electrolyte leads to a 63-fold improvement in the lifetime and achieves an astonishing accumulated capacity of 4 Ah cm^{-2} for Zn (vs. 0.06 Ah cm^{-2} for 3-A_0H_1).

Moreover, Coulombic efficiency (CE) is a critical metric in presenting Zn plating and stripping reversibility.[38] In our study, AN enhanced the CE of Cu||Zn cells from 90.6 % (3-A_0H_1) to 98.6 % (3-A_1H_1) cycled at 1 mA cm^{-2} and 1 mAh cm^{-2} (Figure 2b), indicating an improved Zn reversibility in 3-A_1H_1. Average CEs of Zn plating and stripping on Cu substrate with different mol.% of AN are provided in our Supporting Information (Figure S6, Table S3). In practical use, a competent CE enables a less excessive use of Zn, thereby boosting the cell-level energy density of AZMBs. In fact, a CE as high as 99.9 %, suggested in our previous work, is required to produce a 1000-cycle fictional 120 Wh kg^{-1} AZMB using a controlled Zn utilization of 46 %.[39]

The increased cell overpotential ($\Delta\eta_c$) in 3-A_1H_1 indicates a compromised Zn-ion conductivity. As shown in Figure 2a, Zn plating in 3-A_1H_1 exhibited higher $\Delta\eta_c$ (126.0 mV at cycle 1, 91.3 mV at cycle 100) than in 3-A_0H_1 (57.5 mV in cycle 1, 51.1 mV in cycle 100), indicative of AN exerting suppressing effects on the Zn-ion mobility. There are two possible reasons. (i) The charge status of Zn-ion solvates matters to their migration kinetics in electrolytes. The electrically neutral $[Zn^{2+}(OTf^-)_2(H_2O)_4]$, a dominant solvate form in 3-A_1H_1, migrates relatively slower than the other solvate forms positively charged, such as $[Zn^{2+}(H_2O)_6]$ and $[Zn^{2+}(OTf^-)_1(H_2O)_5]$ in 3-A_0H_1. (ii) Forming aggregates

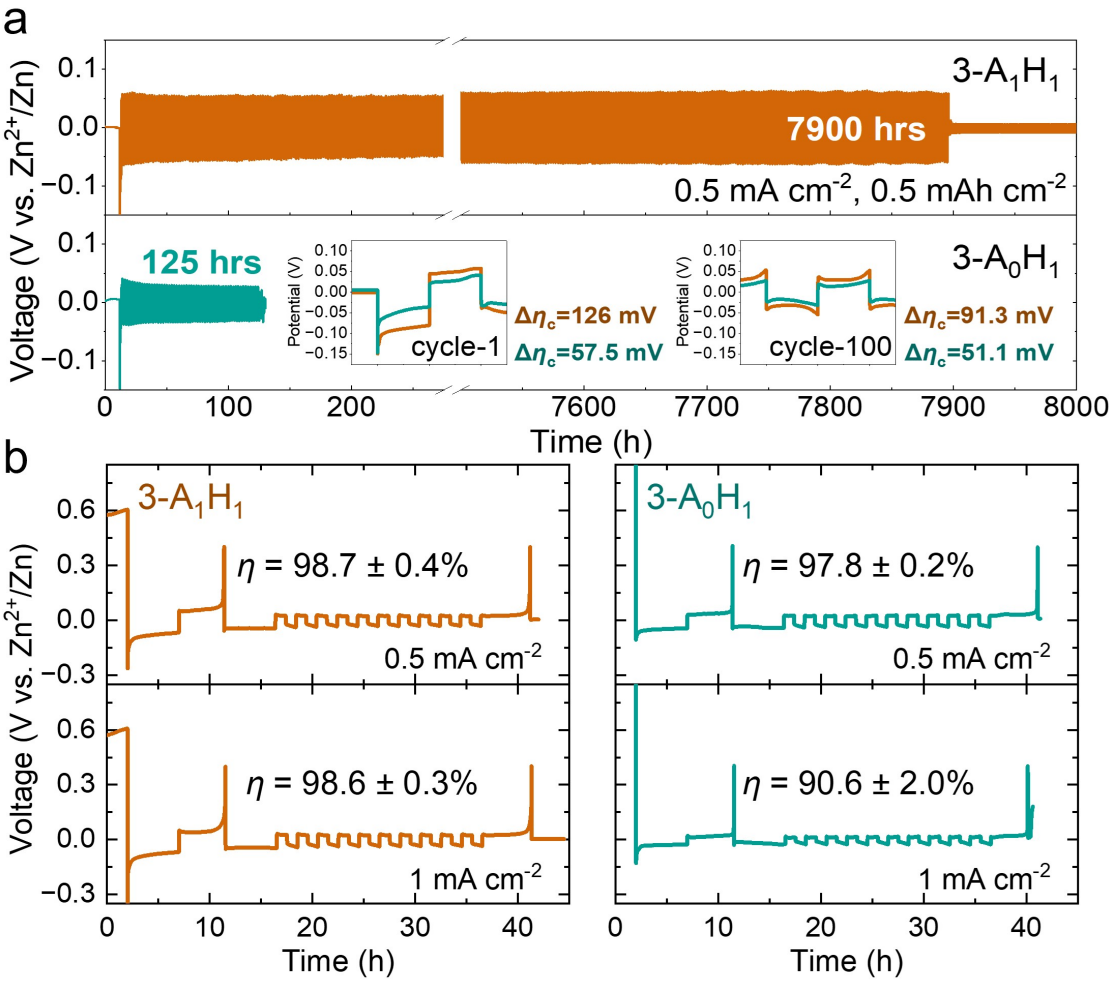

Figure 2. AN effect on the Zn reversibility. (a) Cycling stability in Zn||Zn cells. (b) Coulombic Efficiency (CE) in Cu||Zn cells.

of multiple Zn-ion solvates growing in size also contributes to its sluggish Zn-ion mobility in 3-A_1H_1.

Although several studies have discussed the implications of kinetic factors on Zn electrodeposition behaviors,[40] such as the impact of salt concentration and current density,[41] the "conflicted" result of improved cycling stability and decreased Zn-ion mobility in 3-A_1H_1 indicates that the dendritic Zn growth is more of a thermodynamic consequence than a kinetic one. Despite the sluggish Zn-ion mobility in 3-A_1H_1, this AN-modulated electrolyte suppresses Zn dendrite growth and delays internal short-circuit (Figure 2a). The adsorption energies of AN to different sites of Zn (002) plane are provided in Figure S7. The thermodynamic factor strongly associated with the dendritic Zn growth is later found to be the ample H_2 generation in the non-AN-modulated 3-A_0H_1 electrolyte.

Concurrent analyses of DEMS and OM are employed to understand AN's thermodynamic effect on ameliorating Zn-electrolyte interface instability. As shown in Figure 3a, suppressed gas generation at the Zn|3-A_1H_1 interface, in contrast with the Zn|3-A_0H_1 interface, is observed by OM. In Figure 3b, the gas species in both electrolytes are characterized as H_2 by DEMS. However, the average rate of H_2 generation in 3-A_1H_1 is 2×10^{-4} standard cubic centimeters per minute (sccm), lower than 4×10^{-4} sccm in 3-A_0H_1. Furthermore, while in 3-A_1H_1, little association between H_2 generation and voltage change is presented, the synchrotron fluctuation of detected H_2 signal and voltage in 3-A_0H_1 indicates a relatively low energy barrier of the kinetic-limiting parasitic reaction of H_2O/H_2 alongside the primary reaction of Zn^{2+} deposition than in 3-A_1H_1.[42] To conclude, AN in 3-A_1H_1 is ingrained with a suppressing effect on H_2 generation at the Zn-electrolyte interface during Zn plating and stripping.

The mode of Zn growth alongside bubble walls, a triphasic plane of Zn-electrolyte-H_2, and far-end Zn whiskers detaching from bulk Zn induced by the movement of bubbles is observed (Figure S8). The correlation between H_2 evolution and dendritic Zn growth was observed in previous studies.[43] This phenomenon is due to the bubbles' locally concentrated electric and mass transport fields that introduce significant local heterogeneity into the deposition morphology in the vicinity.[44]

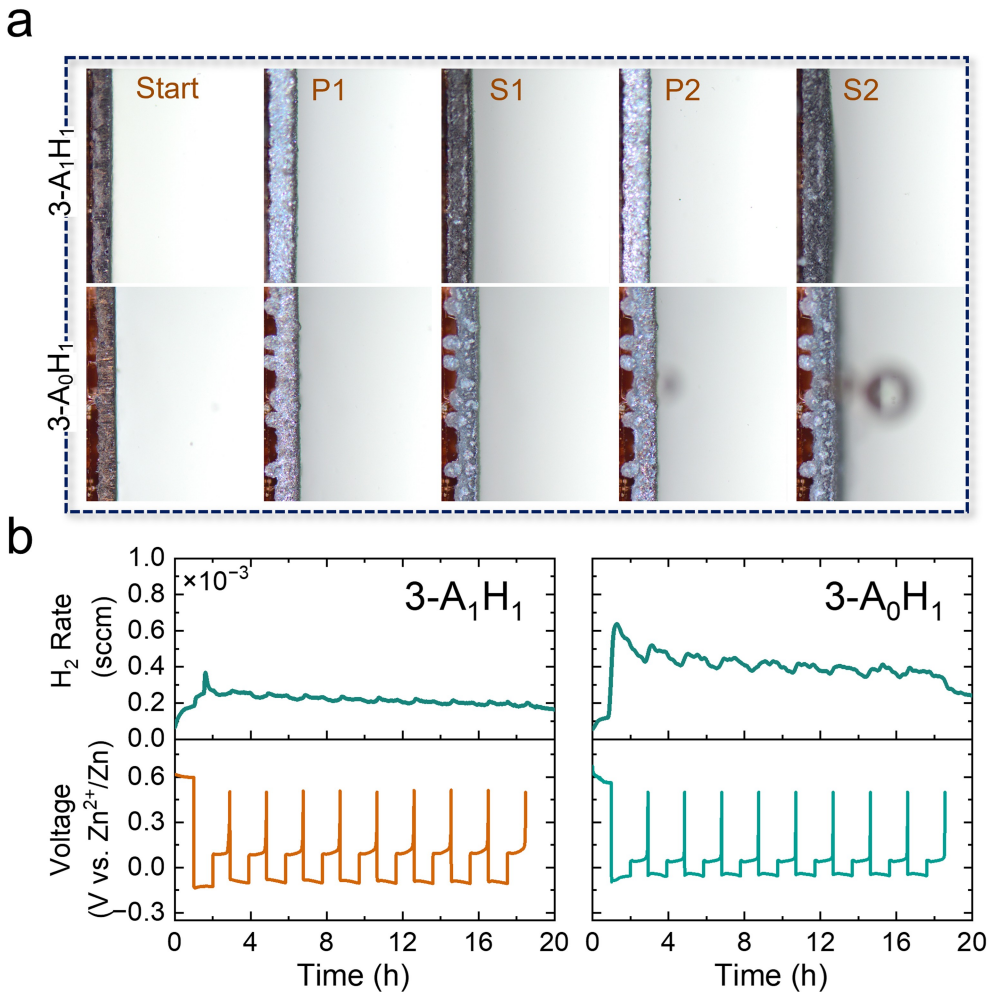

Figure 3. AN effect in H_2 generation. (a) OM images of Zn metals from start to first-cycle plating (P1), first-cycle stripping (S1), second-cycle plating (P2), and second-cycle stripping (S2). (b) Cycling and DEMS results in Cu||Zn at 2 mA cm^{-2} and 2 mAh cm^{-2}.

The Inescapable water activity in AZMBs is intrinsically intertwined with H_2 evolution kinetics. For understanding this phenomenon of AN ameliorating H_2 evolution in AZMBs, rooting in solvation structures remains paramount. Drawing connections to MD simulation result, AN is unable to solvate Zn ions, though, but it can indirectly modulate the solvation structure of Zn ions: $[Zn(H_2O)_6]^{2+}$ remains one of the primary complexes in 3-A_0H_1 in contrast with $[Zn^{2+}(OTf^-)_2(H_2O)_4]$ in 3-A_1H_1. The elevated concentration of "active" water decomposition from $[Zn(H_2O)_6]^{2+}$ exacerbates the H_2 evolution in 3-A_0H_1. Despite the relatively small energy barrier of $[Zn(H_2O)_6]^{2+}$ desolvation in bulky electrolyte (11.6 eV, Figure S9) compared with $[Zn^{2+}(OTf^-)_2(H_2O)_4]$ (19.1 eV) and $[Zn^{2+}(OTf^-)_1(H_2O)_5]$ (16.2 eV), this SSIP-dominated solvate in 3-A_0H_1 in practice leads to sluggish interfacial "desolvation" occurring at the inner Helmholtz plane on the electrode surface, a step requiring a huge amount of energy and widely considered the kinetic-limiting factor among all processes in AZMBs.[45] By contrast, the decreased number of "active" water in the Zn-ion solvates of 3-A_1H_1 ameliorates the parasitic reactions at interface (i.e., H_2 evolution, Zn corrosion and passivation) with a facile desolvation diminishing the tendency of dendritic Zn growth; however, its increased number of anions with negative charges lead to a less than "+2" valence state of the whole Zn-ion solvate, which can result in the aforementioned drawback of sluggish Zn-ion mobility in the bulky electrolyte. Therefore, balancing the number of water and negatively-charged anions in Zn-ion solvates is of great significance in achieving both fast Zn-ion migration and relatively facile desolvation.[46]

AN Reduces V-ion Dissolution and H_2/CO_2 Evolution in Full Cells

The suppressed gas generation in the AN-modulated electrolyte of 3-A_1H_1 on the cathode side occurring at high voltages, for the first time, is characterized as carbon dioxide (CO_2), as shown in Figure 4. The cathodic gas generation of CO_2 in 3-A_0H_1 starts from 2 V; however, in 3-A_1H_1, it occurs at a voltage as high as 2.6 V. The upper ESPW is also improved to 2.6 V in 3-A_1H_1 from 2.5 V in 3-A_0H_1. The detected CO_2, we postulate, is derived from electrochemical corrosion of conductive carbon in the cathode, known as "carbon corrosion," an inherent issue in Zn-air batteries[47] and full cells[48] using carbon cloth as cathode substrate. Theoretically, CO_2/C in aqueous acid electrolyte occurs at 0.208 V vs. SHE (~1 V vs. Zn^{2+}/Zn), close to the reduction-oxidation (redox) potential of V(IV)/V(III) pair (0.34 V vs. SHE, ~1.1 V vs. Zn^{2+}/Zn). Still, experimentally, the sluggish kinetics of C/CO_2 make CO_2 occur at higher voltages than their theoretical redox potentials upon finishing $Zn_{0.5}V_2O_5$/V_2O_5. Despite it being observed that AN suppresses the CO_2 generation in AZMBs, the generation mechanism of CO_2 and consequential implications, such as PH deviation[49] and SEI formation,[50] need to be further studied. According to XRD and XPS results (Figure S10), SEI in 3-A_1H_1 presented a different chemical composition than in 3-A_0H_1.[51] The influence of dissolved gas species (e.g., H_2, O_2, CO_2) on SEI formation has been reported in aqueous LIBs and other systems.[52] However, this phenomenon is yet to be studied in AZMBs.

Figure 5a shows that the capacity of V_2O_5|3-A_1H_1|Zn full cell remained 62 mAh g^{-1} after 1,000 cycles at

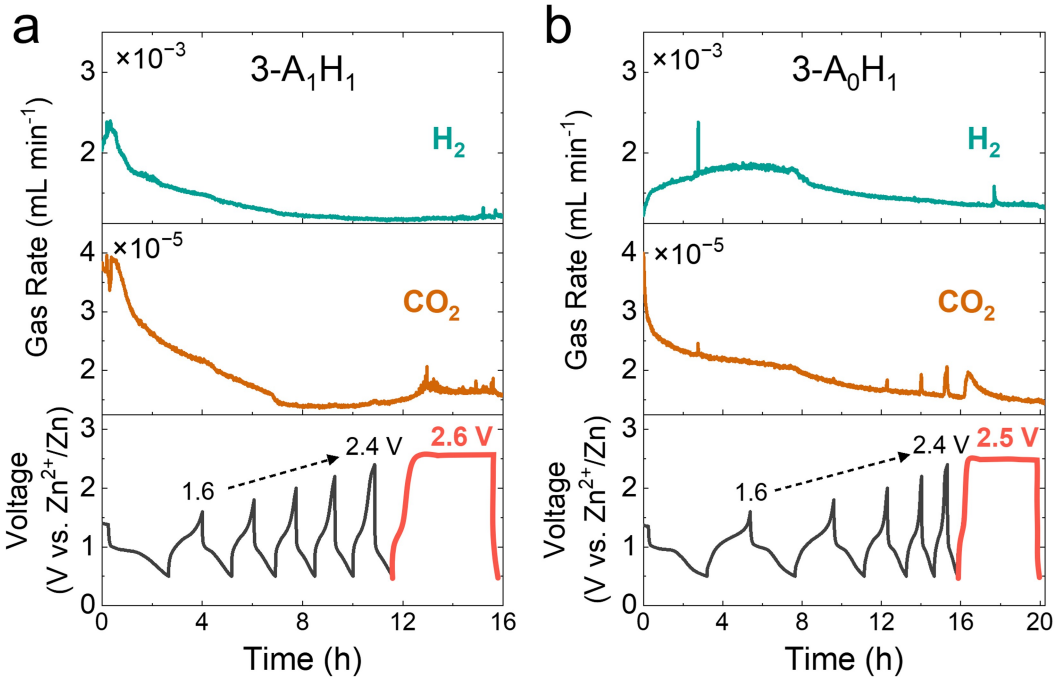

Figure 4. EC-DEMS results in V_2O_5||Zn full cells with (a) 3-A_1H_1 and (b) 3-A_0H_1 cycled at varying cut-off voltages of 1.6 to 2.6 V and current density of 50 mA g^{-1}.

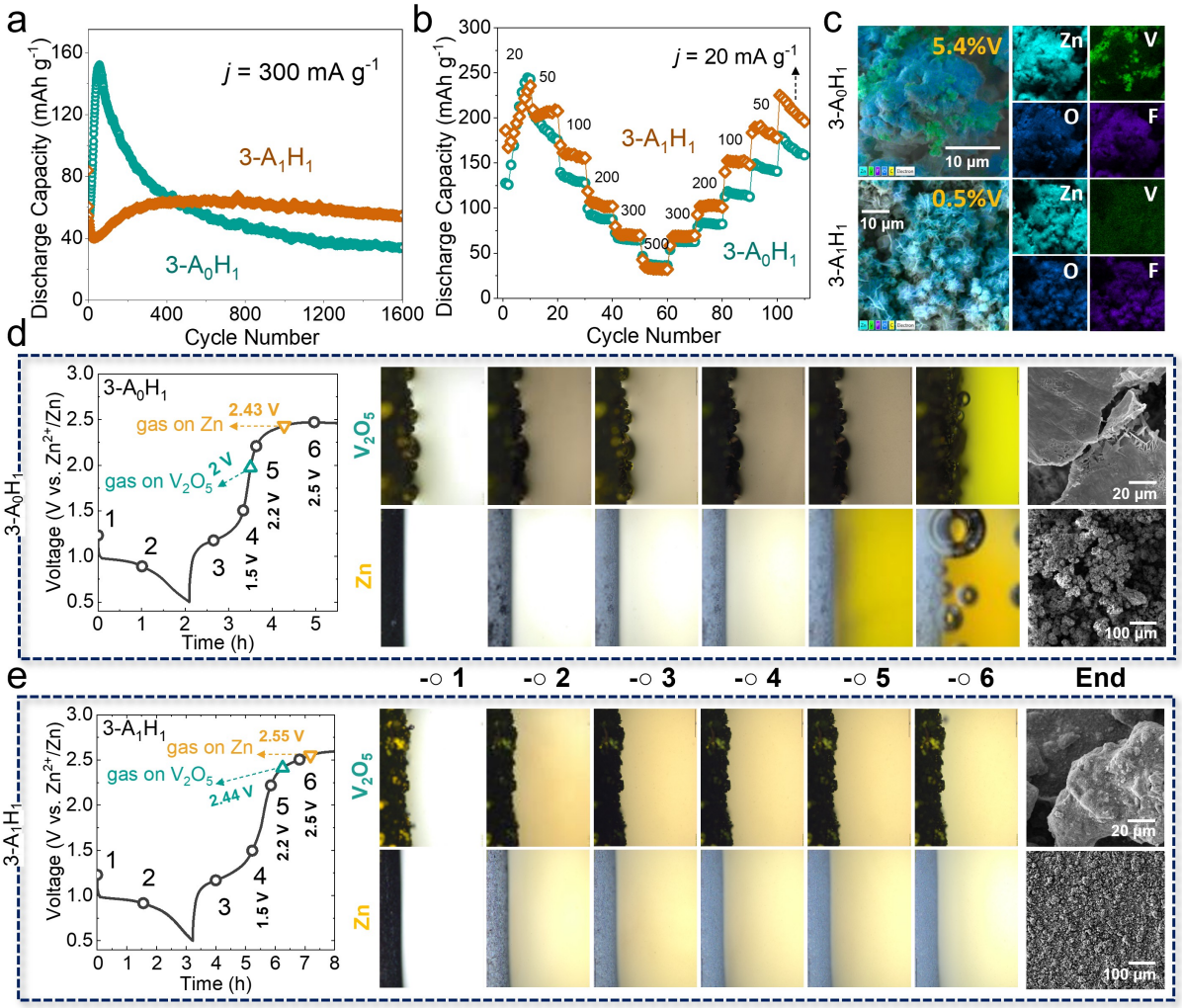

Figure 5. AN effect in $V_2O_5||Zn$ cells. (a) Cycling and (b) rate performance at the voltage of 0.5–1.6 V. (c) Element mapping on post-mortem Zn. (d–e) In situ observation of interfacial reactions of both electrodes during charge and discharge in 3-A_0H_1 and 3-A_1H_1.

300 mA g^{-1} and 0.—1.6 V, in contrast with the drastic capacity decay to 35 mAh g^{-1} of $V_2O_5|3\text{-}A_0H_1|Zn$. Therefore, AN presented an effect of elevating AZMB's capacity retention and elongating cycle life. In fact, the beginning high capacity of $V_2O_5|3\text{-}A_0H_1|Zn$ came from the high reactivity of V_2O_5 in aqueous electrolyte, which, however, did not outcompete the as-reactive parasitic reactions. During the rate test (Figure 5b), V_2O_5 in the AN-modulated electrolyte demonstrated higher capacity of 205, 160, 102, 71 mAh g^{-1} than the 185, 130, 88, 75 mAh g^{-1} in 3-A_0H_1 at varying current density of 50, 100, 200, 300 mA g^{-1}, respectively, which confirms the aforementioned effectiveness of AN additive in improving the kinetics of Zn-ion desolvation in full cells.

We conducted SEM and EDS analysis on the post-mortem Zn metal cycling in both electrolytes. Unexpectedly, apparent V deposits on Zn are observed: the vanadium (V) concentration obtained from EDS is reduced from 5.4 wt % for A_0H_1 to 0.5 wt % for 3-A_1H_1 (Figure 5c). In fact, the same pattern is observed in their diluted sister-electrolytes: 14.0 wt % for 0.3-A_0H_1 to 8.6 wt % for 0.3-A_1H_1 (Figure S11). We further conducted XPS analysis and found that the post-mortem cathode cycled in 3-A_0H_1 presented 0 atomic percent (at%) of V and 4.0 at.% of Zn, suggesting strong V dissolution and irreversible Zn deintercalation (Figure S12), while in 3-A_1H_1, the cycled cathode preserved 11.4 at% of V and only 1.0 at% of irreversible Zn, together with the high-resolution V2p spectra, where +5 valence state V were most preserved (61 %), suggesting AN's suppressing effect in cathode dissolution. XPS on post-mortem Zn suggested that the V deposit on Zn cycled in 3-A_1H_1 (0.6 at%) is less than that on Zn cycled in 3-A_0H_1 (0.8 at%, Figure S13). These observations indicate an effect of AN in suppressing V-ion dissolution, migration, and deposition. The consequences are multifaceted. (i) The dissolution of V centers comes with a structural collapse of interfacial V_2O_5 crystals, leading to irreversible capacity loss of the cathode. (ii) After V ions migrate to the anode surface, the random electrodeposition of V-compounds on Zn metal can have detrimental effects on Zn, such as

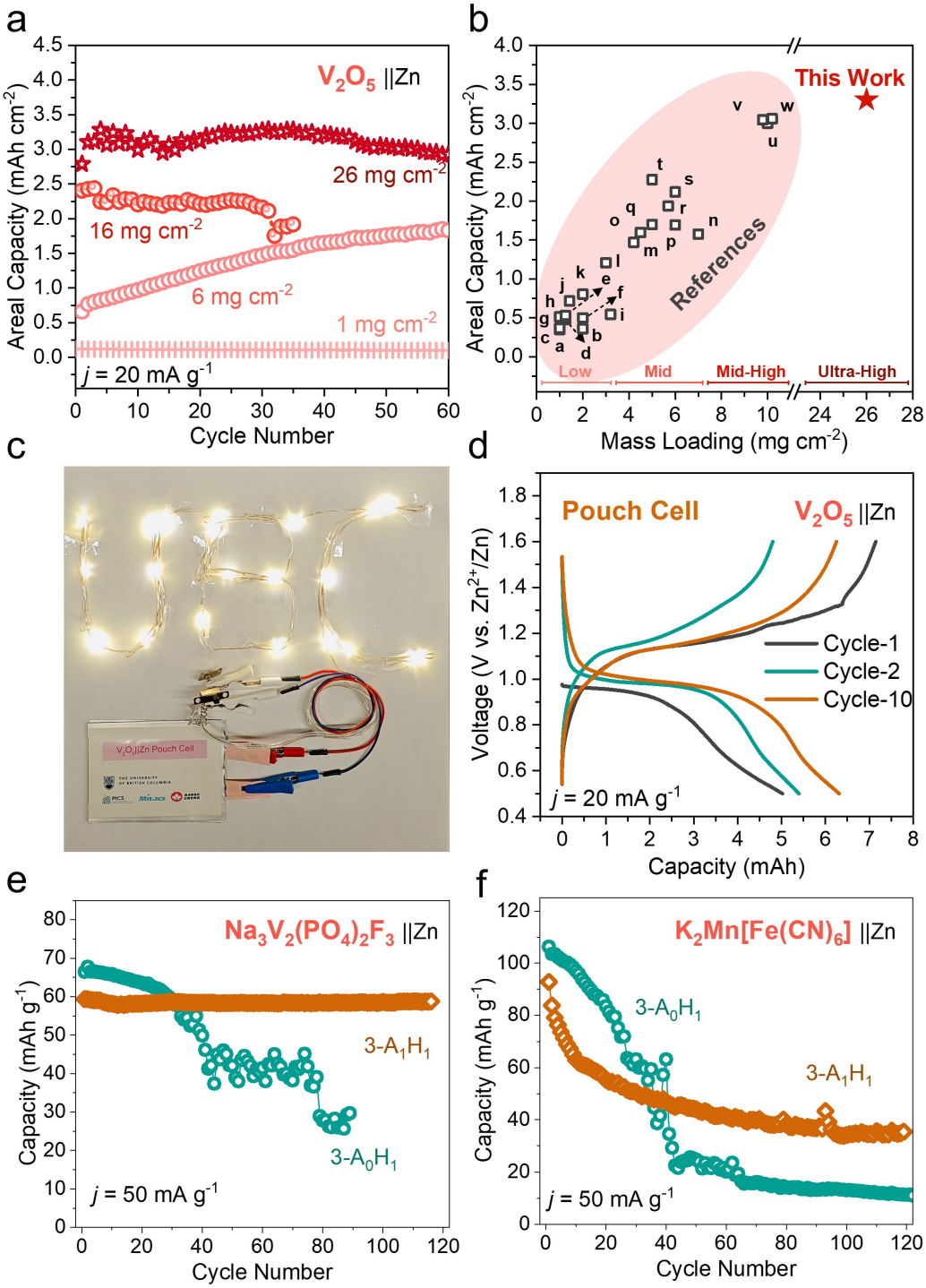

Figure 6. (a) Cycling stability of high-loading V_2O_5 cathodes with the 3-A_1H_1 electrolyte after a 100-cycle pre-cycling. (b) Comparison of this work with references 59. (c) A demonstration of connecting three 2.5×4 cm^2 V_2O_5 | 3-A_1H_1 | Zn pouch cells in series. (d) Charge and discharge profiles of a dry-film V_2O_5 | 3-A_1H_1 | Zn pouch cell. Effectiveness of AN additive in (e) $Na_3V_2(PO_4)_2F_3$ | | Zn and (f) $K_2[MnFe(CN)_6]$ | | Zn cells.

reduced effective area of Zn,[53] inhomogeneous Zn deposition,[54] and thereby irreversible Zn loss. This presents an effect akin to the electrochemical "crosstalk" reported in lithium-ion batteries, where TM-ion dissolution,[55] during high-voltage cycling, leads to heavy separator degradation and high-degree SEI localization.[56] All of the above motivates us to use in situ OM to further observe the cause of V deposits.

As shown in Figure 5d, the V_2O_5-side interfacial electrolyte of 3-A_0H_1 started presenting an umber color at the beginning of discharge and experienced a drastic color change at the vicinity of point 5 (2.5 V vs. Zn^{2+}/Zn) from

olive to lime and then to orange (Video S1), suggesting a drastic V-ion dissolution and high activity of parasitic V-ion redox reactions, while a more subdued dissolution and change of interfacial electrolyte color is presented in 3-A_1H_1 (Figure 5e, Video S2). For the Zn-side interface with 3-A_0H_1, V ions migrate to the Zn metal and start showing a yellow dye at 1.55 V, followed by a "sandstorm"-like phenomenon at 2.20 V (Video S1), suggesting an aroused vortex from a bombardment of fast parasitic reactions at the interface, while there is no such observation in 3-A_1H_1. The H_2 generation on the Zn side occurs at 2.43 V in 3-A_0H_1 in contrast with 2.55 V in 3-A_1H_1, indicating better thermodynamic stability of the interface between Zn and the AN-modulated electrolyte. This could be related to the aforementioned varying solvation-sheath composition and desolvation energy barrier at the inner Helmholtz plane in electrolytes with different ratios of CIPs and SSIPs.[57] The V_2O_5-side gas generation occurs at 2.00 V in 3-A_0H_1, while the gas-initiation voltage in 3-A_1H_1 is elevated to 2.44 V. This gas may correspond to the CO_2 previously detected by DEMS (Figure 4). The "cracked" surface of the post-mortem V_2O_5 cycled in 3-A_0H_1 also indicated severe cathodic gas generation, while in 3-A_1H_1, the cycled V_2O_5 still presented regular morphology (Figure S14–15). For the post-mortem Zn, mossy-like Zn deposits were observed with 3-A_0H_1, while Zn cycled in 3-A_1H_1 presented commendable homogeneity (Figure S16).

In summary, AN presented a suppressing effect towards cathode dissolution, V-ion crosstalk, and gas-evolving parasitic reactions. Consequently, the structural stability of both Zn anode and V_2O_5 electrodes was improved with 3-A_1H_1.

AN Enables High Loading and High Areal Capacity

High areal capacity is a crucial metric for practical battery applications. However, electrolyte wetting becomes a limiting factor for high-mass-loading cathode, such as in Li–S batteries.[58] Figure S17a showed that using the conventional 3-A_0H_1 electrolyte, the capacity deterioration of V_2O_5|3-A_0H_1|Zn as cathode loading increases was apparent. However, AN has a lower viscosity than water, indicating good wettability of 3-A_1H_1.

The solvent-free dry-film technique is gaining attention for its ability to prevent pollution from toxic solvents, prevent undesired side reactions between solvent and active materials, and reduce the cost of materials and recycling. In addition, it is a facile preparation method for high-loading electrodes and high areal capacity batteries against the delamination problem found in wet-chemistry-prepared high-loading electrodes. Figure 6a and Figure S17b–c show that 3-A_1H_1 works well with high-loading cathodes (the 16 and 26 mg cm^{-2} are prepared by dry-film method, the 1 and 6 mg cm^{-2} are prepared by regular doctor-blading method, Supporting Information), suggesting good permeability of the AN-modulated electrolyte with the cathode.

Compared with reported V_2O_5||Zn cells,[59] this work achieved an exceptional areal capacity of 3.3 mAh cm^{-2}, as shown in Figure 6b, using a 26 mg cm^{-2} loaded V_2O_5|3-A_1H_1|Zn configuration. Furthermore, by connecting three V_2O_5|3-A_1H_1|Zn pouch cells in parallel, the LED strip, designed to operate at a rated voltage of 3 V, was effectively illuminated, as depicted in Figure 6c. Utilizing the 3-A_1H_1 electrolyte enabled the AZMB pouch cell to consistently maintain a discharge plateau around 1 V (Figure 6d). The efficacy of 3-A_1H_1 extends to various cathode types, such as $Na_3V_2(PO_4)_2F_3$ (polyanion) and $K_2[MnFe(CN)_6]$ (Prussian blue analog), as illustrated in Figure 5e–f and Figure S18.

Conclusions

This study constructed a 3.3 mAh cm^{-2} AZMB using an AN-modulated electrolyte and a 26 mg cm^{-2} V_2O_5 dry-film cathode. The AN additive reduced Zn-H_2O coordination in Zn-ion solvation sheath, promoting facile desolvation kinetics. This leads to multi-dimensional benefits: (i) a suppressing effect on H_2 and CO_2 gas evolution, (ii) a suppressing effect on V-ion dissolution and its deposition on Zn, (iii) a promoting effect on Zn electrodeposition homogeneity. Electrochemically, additive of AN increased the Zn||Zn cycle life by 63 times, achieving an accumulated areal capacity of 4 Ah cm^{-2}, and improved the capacity retention of V_2O_5||Zn, with its capacity remaining at 62 mAh g^{-1} after 1000 cycles at 300 mA g^{-1}. The guaranteed high-loading cycling performance with AN additive is ascribed to the permeability of the electrolyte. The examination of parasitic reactions offers valuable insights for future research endeavors. Future studies should take a comprehensive approach by (i) exploring the advantages and disadvantages of these gaseous byproducts in AZMBs, along with their potential crosstalk mechanisms; (ii) delving into the intricacies of V-dissolution/deposition crosstalk and examining its ripple effects on gas production and Zn deposition homogeneity on the anode side.

Acknowledgements

This work is supported by the Nature Sciences and Engineering Research Council of Canada (NSERC), Canada Foundation for Innovation (CFI), BC Knowledge Development Fund (BCKDF), the Daniel Family Foundation, and the University of British Columbia (UBC). We extend our appreciation to Ieva Zigg for her assistance with FTIR analysis and for the utilization of the ATR-IR facility at the chemistry department teaching lab, UBC Okanagan. We express our gratitude for the access to the XPS facility at nanoFAB, University of Alberta. Special thanks are due to Dr. Matthew L. Brown, WD lab in UBC Okanagan, for his valuable support in conducting XRD tests.

Conflict of Interest

The authors declare no competing financial interest.

Data Availability Statement

The data that support the findings of this study are available from the corresponding author upon reasonable request.

Keywords: electrolyte additive · gas evolution suppression · Zn-dendrite mitigation · Vanadium dissolution alleviation · Zn metal anode · aqueous Zn-metal batteries

[1] a) D. Kundu, B. D. Adams, V. Duffort, S. H. Vajargah, L. F. Nazar, *Nat. Energy* **2016**, *1*; b) H. Pan, Y. Shao, P. Yan, Y. Cheng, K. S. Han, Z. Nie, C. Wang, J. Yang, X. Li, P. Bhattacharya, K. T. Mueller, J. Liu, *Nat. Energy* **2016**, *1*.

[2] Y. Liu, X. Lu, F. Lai, T. Liu, P. R. Shearing, I. P. Parkin, G. He, D. J. L. Brett, *Joule* **2021**, *5*, 2845–2903.

[3] J. Yan, E. H. Ang, Y. Yang, Y. Zhang, M. Ye, W. Du, C. C. Li, *Adv. Funct. Mater.* **2021**, *31*.

[4] a) X. Lu, Z. Liu, A. Amardeep, Z. Wu, L. Tao, K. Qu, H. Sun, Y. Liu, J. Liu, *Angew. Chem. Int. Ed. Engl.* **2023**, *62*, e202307475; b) L. Geng, J. Meng, X. Wang, C. Han, K. Han, Z. Xiao, M. Huang, P. Xu, L. Zhang, L. Zhou, *Angew. Chem. Int. Ed.* **2022**, *61*, e202206717.

[5] L. Yu, J. Huang, S. Wang, L. Qi, S. Wang, C. Chen, *Adv. Mater.* **2023**, *35*, e2210789.

[6] N. Wang, X. Dong, B. Wang, Z. Guo, Z. Wang, R. Wang, X. Qiu, Y. Wang, *Angew. Chem. Int. Ed. Engl.* **2020**, *59*, 14577–14583.

[7] N. Chang, T. Li, R. Li, S. Wang, Y. Yin, H. Zhang, X. Li, *Energy Environ. Sci.* **2020**, *13*, 3527–3535.

[8] Z. Ma, J. Chen, J. Vatamanu, O. Borodin, D. Bedrov, X. Zhou, W. Zhang, W. Li, K. Xu, L. Xing, *Energy Storage Mater.* **2022**, *45*, 903–910.

[9] S. Hou, X. Ji, K. Gaskell, P.-f. Wang, L. Wang, J. Xu, R. Sun, O. Borodin, C. Wang, *Science* **2021**, *374*, 172–178.

[10] Q. Zhao, S. Stalin, L. A. Archer, *Joule* **2021**, *5*, 1119–1142.

[11] Y. Zhang, G. Wan, N. H. C. Lewis, J. Mars, S. E. Bone, H.-G. Steinrück, M. R. Lukatskaya, N. J. Weadock, M. Bajdich, O. Borodin, A. Tokmakoff, M. F. Toney, E. J. Maginn, *ACS Energy Lett.* **2021**, *6*, 3458–3463.

[12] J. Wang, J. X. Tian, G. X. Liu, Z. Z. Shen, R. Wen, *Small Methods* **2023**, 2300392.

[13] N. Zhang, F. Cheng, Y. Liu, Q. Zhao, K. Lei, C. Chen, X. Liu, J. Chen, *J. Am. Chem. Soc.* **2016**, *138*, 12894–12901.

[14] S. Chen, Q. Nian, L. Zheng, B.-Q. Xiong, Z. Wang, Y. Shen, X. Ren, *J. Mater. Chem. A* **2021**, *9*, 22347–22352.

[15] H. Li, S. Guo, H. Zhou, *Energy Storage Mater.* **2023**, *56*, 227–257.

[16] W. Deng, Z. Xu, X. Wang, *Energy Storage Mater.* **2022**, *52*, 52–60.

[17] D. Feng, F. Cao, L. Hou, T. Li, Y. Jiao, P. Wu, *Small* **2021**, *17*, e2103195.

[18] S. Liu, J. Mao, W. K. Pang, J. Vongsvivut, X. Zeng, L. Thomsen, Y. Wang, J. Liu, D. Li, Z. Guo, *Adv. Funct. Mater.* **2021**, *31*, 2104281.

[19] R. Qin, Y. Wang, M. Zhang, Y. Wang, S. Ding, A. Song, H. Yi, L. Yang, Y. Song, Y. Cui, *Nano Energy* **2021**, *80*, 105478.

[20] X. Shi, J. Xie, J. Wang, S. Xie, Z. Yang, X. Lu, *Nat. Commun.* **2024**, *15*, 302.

[21] L. Yuan, J. Hao, B. Johannessen, C. Ye, F. Yang, C. Wu, S.-X. Dou, H.-K. Liu, S.-Z. Qiao, *eScience* **2023**, *3*, 100096.

[22] J. Xie, Z. Liang, Y. C. Lu, *Nat. Mater.* **2020**, *19*, 1006–1011.

[23] D. Dong, J. Xie, Z. Liang, Y.-C. Lu, *ACS Energy Lett.* **2021**, *7*, 123–130.

[24] F. Ming, Y. Zhu, G. Huang, A. H. Emwas, H. Liang, Y. Cui, H. N. Alshareef, *J. Am. Chem. Soc.* **2022**, *144*, 7160–7170.

[25] L. Miao, R. Wang, S. Di, Z. Qian, L. Zhang, W. Xin, M. Liu, Z. Zhu, S. Chu, Y. Du, N. Zhang, *ACS Nano* **2022**, *16*, 9667–9678.

[26] D. Kundu, S. Hosseini Vajargah, L. Wan, B. Adams, D. Prendergast, L. F. Nazar, *Energy Environ. Sci.* **2018**, *11*, 881–892.

[27] J. Shi, K. Xia, L. Liu, C. Liu, Q. Zhang, L. Li, X. Zhou, J. Liang, Z. Tao, *Electrochim. Acta* **2020**, *358*.

[28] C. Meng, W. He, Z. Kong, Z. Liang, H. Zhao, Y. Lei, Y. Wu, X. Hao, *Chem. Eng. J.* **2022**, *450*.

[29] H. Zhao, Q. Fu, X. Luo, X. Wu, S. Indris, M. Bauer, Y. Wang, H. Ehrenberg, M. Knapp, Y. Wei, *Energy Storage Mater.* **2022**, *50*, 464–472.

[30] X. Song, H. He, M. H. Aboonasr Shiraz, H. Zhu, A. Khosrozadeh, J. Liu, *Chem. Commun. (Camb.)* **2021**, *57*, 1246–1249.

[31] J. Zhao, J. Zhang, W. Yang, B. Chen, Z. Zhao, H. Qiu, S. Dong, X. Zhou, G. Cui, L. Chen, *Nano Energy* **2019**, *57*, 625–634.

[32] Z. Zhao, J. Zhao, Z. Hu, J. Li, J. Li, Y. Zhang, C. Wang, G. Cui, *Energy Environ. Sci.* **2019**, *12*, 1938–1949.

[33] L. Ma, Q. Li, Y. Ying, F. Ma, S. Chen, Y. Li, H. Huang, C. Zhi, *Adv. Mater.* **2021**, *33*, e2007406.

[34] P. Xiao, X. Yun, Y. Chen, X. Guo, P. Gao, G. Zhou, C. Zheng, *Chem. Soc. Rev.* **2023**, *52*, 5255–5316.

[35] E. Pace, L. J. Noe, *J. Chem. Phys.* **1968**, *49*, 5317–5325.

[36] J. Reedijk, A. Zuur, W. Groeneveld, *Recueil des Travaux Chimiques des Pays-Bas* **1967**, *86*, 1127–1137.

[37] R. Kumar, J. P. Sharma, S. S. Sekhon, *Eur. Polym. J.* **2005**, *41*, 2718–2725.

[38] L. Ma, M. A. Schroeder, O. Borodin, T. P. Pollard, M. S. Ding, C. Wang, K. Xu, *Nat. Energy* **2020**, *5*, 743–749.

[39] Z. Wu, Y. Li, J. Liu, *Small Methods* **2023**, 2300660.

[40] Q. Li, A. Chen, D. Wang, Y. Zhao, X. Wang, X. Jin, B. Xiong, C. Zhi, *Nat. Commun.* **2022**, *13*, 3699.

[41] X. Ye, M. Saqib, J. Mao, G. Li, R. Hao, *Cell Reports Physical Science* **2021**, *2*.

[42] J. W. S. K. Wippermann, R. Kessel, J. Penninger, *Corros. Sci.* **1991**.

[43] a) W. Tsai, P. Hsu, Y. Hwu, C. Chen, L. Chang, J. Je, H. Lin, A. Groso, G. Margaritondo, *Nature* **2002**, *417*, 139–139; b) G. Chang, S. Liu, Y. Fu, X. Hao, W. Jin, X. Ji, J. Hu, *Adv. Mater. Interfaces* **2019**, *6*.

[44] J. Zheng, L. A. Archer, *Sci. Adv.* **2021**.

[45] Y. Li, C. B. Musgrave, M. Y. Yang, M. M. Kim, K. Zhang, M. Tamtaji, Y. Cai, T. W. Tang, J. Wang, B. Yuan, W. A. Goddard, Z. Luo, *Adv. Energy Mater.* **2023**.

[46] J. Cao, Y. Sun, D. Zhang, D. Luo, L. Zhang, R. Chanajaree, J. Qin, X. Yang, J. Lu, *Adv. Energy Mater.* **2023**.

[47] S. Zhao, T. Liu, J. Wang, I. Temitope Bello, Y. Zuo, M. Wei, K. Wang, K. K. S. Lau, M. Ni, *Chem. Eng. J.* **2022**, *450*.

[48] J. Zhao, Z. Tu, S. H. Chan, *J. Power Sources* **2021**, *488*.

[49] X. Liu, H. Euchner, M. Zarrabeitia, X. Gao, G. A. Elia, A. Gross, S. Passerini, *ACS Energy Lett.* **2020**, *5*, 2979–2986.

[50] a) J. Yue, J. Zhang, Y. Tong, M. Chen, L. Liu, L. Jiang, T. Lv, Y. S. Hu, H. Li, X. Huang, L. Gu, G. Feng, K. Xu, L. Suo, L. Chen, *Nat. Chem.* **2021**, *13*, 1061–1069; b) D. B. Thornton, B. J. Davies, S. B. Scott, A. Aguadero, M. P. Ryan, I. E. L. Stephens, *Angew. Chem.* **2023**, e202315357.

[51] a) T. N. Ramesh, T. L. Madhu, *International Journal of Inorganic Chemistry* **2015**, *2015*, 1–11; b) M. Yang, Z. Yan, J. Xiao, W. Xin, L. Zhang, H. Peng, Y. Geng, J. Li, Y. Wang, L. Liu, Z. Zhu, *Angew. Chem. Int. Ed. Engl.* **2022**, *61*, e202212666.

[52] a) L. Suo, D. Oh, Y. Lin, Z. Zhuo, O. Borodin, T. Gao, F. Wang, A. Kushima, Z. Wang, H. C. Kim, Y. Qi, W. Yang, F. Pan, J. Li, K. Xu, C. Wang, *J. Am. Chem. Soc.* **2017**, *139*, 18670–18680; b) M. Huang, X. Wang, J. Wang, J. Meng, X. Liu,

Q. He, L. Geng, Q. An, J. Yang, L. Mai, *Angew. Chem.* **2023**, *135*, e202308961.
[53] F.-D. Yu, Z.-J. Yi, R.-Y. Li, W.-H. Lin, J. Chen, X.-Y. Chen, Y.-M. Xie, J.-H. Wu, Z. Lan, L.-F. Que, B.-S. Liu, H. Luo, Z.-B. Wang, *J. Energy Chem.* **2023**.
[54] Y. Song, L. Wang, L. Sheng, M. Zhang, H. Liang, D. Ren, H. Cui, H. Zhang, H. Xu, X. He, *Energy Storage Mater.* **2023**, *63*.
[55] L. Rynearson, C. Antolini, C. Jayawardana, M. Yeddala, D. Hayes, B. L. Lucht, *Angew. Chem. Int. Ed. Engl.* **2023**, e202317109.
[56] R. Sim, L. Su, A. Dolocan, A. Manthiram, *Adv. Mater.* **2023**, e2311573.
[57] C. Yan, H. R. Li, X. Chen, X. Q. Zhang, X. B. Cheng, R. Xu, J. Q. Huang, Q. Zhang, *J. Am. Chem. Soc.* **2019**, *141*, 9422–9429.
[58] T. Zerrin, R. Shang, B. Dong, E. C. Aguilar, J. Malvin, M. Ozkan, C. S. Ozkan, *Nano Energy* **2022**, *104*.
[59] a) Z. Qi, T. Xiong, T. Chen, W. Shi, M. Zhang, Z. W. J. Ang, H. Fan, H. Xiao, W. S. V. Lee, J. Xue, *J. Alloys Compd.* **2021**, *870*, 159403; b) X. Chen, L. Wang, H. Li, F. Cheng, J. Chen, *J. Energy Chem.* **2019**, *38*, 20–25; c) H. Geng, M. Cheng, B. Wang, Y. Yang, Y. Zhang, C. C. Li, *Adv. Funct. Mater.* **2020**, *30*, 1907684; d) Y. Kim, Y. Park, M. Kim, J. Lee, K. J. Kim, J. W. Choi, *Nat. Commun.* **2022**, *13*, 2371; e) S. Liu, H. Zhu, B. Zhang, G. Li, H. Zhu, Y. Ren, H. Geng, Y. Yang, Q. Liu, C. C. Li, *Adv. Mater.* **2020**, *32*, 2001113; f) L. Wang, K.-W. Huang, J. Chen, J. Zheng, *Sci. Adv.* **2019**, *5*, eaax4279; g) Y. Lu, T. Zhu, W. van den Bergh, M. Stefik, K. Huang, *Angew. Chem.* **2020**, *132*, 17152–17159; h) D. Jia, Z. Shen, Y. Lv, Z. Chen, H. Li, Y. Yu, J. Qiu, X. He, *Adv. Funct. Mater.* **2023**, 2308319; i) P. Senguttuvan, S. D. Han, S. Kim, A. L. Lipson, S. Tepavcevic, T. T. Fister, I. D. Bloom, A. K. Burrell, C. S. Johnson, *Adv. Energy Mater.* **2016**, *6*, 1600826; j) M. S. Javed, H. Lei, Z. Wang, B.-t. Liu, X. Cai, W. Mai, *Nano Energy* **2020**, *70*, 104573; k) J. J. Ye, P. H. Li, H. R. Zhang, Z. Y. Song, T. Fan, W. Zhang, J. Tian, T. Huang, Y. Qian, Z. Hou, *Adv. Funct. Mater.* **2023**, *33*, 2305659; l) J. Li, K. McColl, X. Lu, S. Sathasivam, H. Dong, L. Kang, Z. Li, S. Zhao, A. G. Kafizas, R. Wang, *Adv. Energy Mater.* **2020**, *10*, 2000058; m) X. Liang, L. Yan, W. Li, Y. Bai, C. Zhu, Y. Qiang, B. Xiong, B. Xiang, X. Zou, *Nano Energy* **2021**, *87*, 106164; n) J. Ren, P. Hong, Y. Ran, B. Wang, T. Chen, Y. Wang, *Electrochim. Acta* **2022**, *415*, 140265; o) N. Zhang, M. Jia, Y. Dong, Y. Wang, J. Xu, Y. Liu, L. Jiao, F. Cheng, *Adv. Funct. Mater.* **2019**, *29*, 1807331; p) D. Kundu, B. D. Adams, V. Duffort, S. H. Vajargah, L. F. Nazar, *Nat. Energy* **2016**, *1*, 1–8; q) M. Wang, J. Ma, Y. Meng, J. Sun, Y. Yuan, M. Chuai, N. Chen, Y. Xu, X. Zheng, Z. Li, *Angew. Chem. Int. Ed.* **2023**, *62*, e202214966; r) C. Xia, J. Guo, P. Li, X. Zhang, H. N. Alshareef, *Angew. Chem.* **2018**, *130*, 4007–4012; s) F. Ming, H. Liang, Y. Lei, S. Kandambeth, M. Eddaoudi, H. N. Alshareef, *ACS Energy Lett.* **2018**, *3*, 2602–2609; t) N. Zhang, Y. Dong, M. Jia, X. Bian, Y. Wang, M. Qiu, J. Xu, Y. Liu, L. Jiao, F. Cheng, *ACS Energy Lett.* **2018**, *3*, 1366–1372; u) X. Wang, Y. Li, S. Wang, F. Zhou, P. Das, C. Sun, S. Zheng, Z. S. Wu, *Adv. Energy Mater.* **2020**, *10*, 2000081; v) S. Linghu, J. Ye, K. Deng, P. Liu, Y. Zhong, T. You, W. Tian, J. Ji, *J. Power Sources* **2024**, *592*, 233922; w) D. Zhao, X. Wang, W. Zhang, Y. Zhang, Y. Lei, X. Huang, Q. Zhu, J. Liu, *Adv. Funct. Mater.* **2023**, *33*, 2211412.

Manuscript received: January 31, 2024
Accepted manuscript online: March 8, 2024
Version of record online: April 5, 2024

Research Articles

Batteries

Z. Wu, Y. Li, A. Amardeep, Y. Shao, Y. Zhang, J. Zou, L. Wang, J. Xu, D. Kasprzak, E. J. Hansen, J. Liu* _____ **e202402206**

Unveiling the Mysteries: Acetonitrile's Dance with Weakly-Solvating Electrolytes in Shaping Gas Evolution and Electrochemical Performance of Zinc-ion Batteries

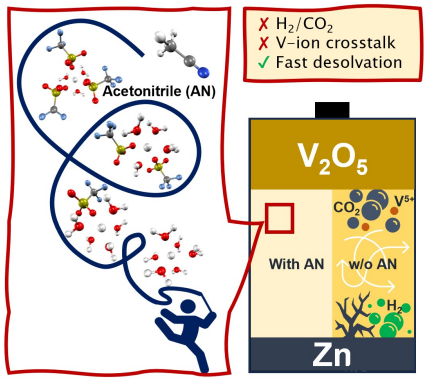

Acetonitrile electrolyte additive is found to delay hydrogen (H_2) and carbon dioxide (CO_2) evolution reactions in aqueous Zn-metal batteries (AZMBs). It also suppresses vanadium (V) dissolution, or V-ion crosstalk, from the vanadium pentoxide (V_2O_5) cathode. Practically, acetonitrile-added electrolyte enabled a high and stable areal capacity of 3.3 mAh cm^{-2} using a 26 mg cm^{-2} V_2O_5 dry-film cathode.